A HIGH FIDELITY WAVE MAKER BASED ON MULTI-MOMENT FINITE VOLUME FORMULATION AND THINC METHOD

ZHIHANG ZHANG[1], XIZENG ZHAO[2], BIN XIE[3]

[1]*Ocean college, Zhejiang University, lokikerry@zju.edu.cn*

[2]*Ocean college, Zhejiang University, xizengzhao@zju.edu.cn*

[3]*School of Naval Architecture, Shanghai Jiaotong University, xie.b.aa@sjtu.edu.cn*

Keywords: *Free-surface waves, numerical dissipation, phase shift, interFoam solver, third-order accurate model*

Second-order accurate numerical methods underpin the majority of industrial CFD solvers as well as the open-source CFD library OpenFOAM. Based on these methods, wave makers are expected to suffer from excessive numerical viscosity, resulting in notable dissipation and reduction in wave energy even for zero physical viscosity. Commercial software STAR-CCM+ and open-source solver interFoam(a multiphase solver within OpenFOAM) are widely used for simulations of free-surface waves in oceanographic engineering and coastal engineering. Simulations of regular-wave propagation with these two solvers show that the results are sensitive to temporal and spatial discretizations [1] [2], indicating that satisfactory results are promised merely when grids and time steps are refined enough using these numerical solvers. But refining grids and time steps leads to increase in computational cost. The increase could be unaffordable for some cases, e.g. those involve short-period waves as the relatively higher frequency causes greater numerical dissipation.

To overcome this problem in numerical investigations, a wave maker based on third-order accurate VPM(volume-average/point-value multi-moment) scheme [3] and THINC/QQ method(the THINC method with quadratic surface representation and Gaussian quadrature) [4] is presented in this study. A mass source function [5] and a sponge layer [6] are embedded into this two-dimensional Navier-Stokes model for wave generation and absorption respectively. Numerical simulations of regular waves with different time steps and grid resolutions are carried out with the present model and interFoam solver for comparison. It is demonstrated that with interFoam solver, generated wave trains encounter a significant loss of wave hight along the propagation direction, in addition, a phase shift is produced due to a change in wave period and wavelength. While the wave maker based on the present model produces high-fidelity results, which show a fairly trifling loss of wave height and negligible phase shift.

The rest of this abstract is organized as follows. After a brief description of governing equations, the solution procedures for both solvers and the numerical setups are given. The simulation results with both solvers are presented and compared to verify the performance of the present solver. This abstract is ended with conclusion remarks and future work.

In this study, the incompressible two-fluid flows with moving interface are solved based on the one-fluid model. The Navier-Stokes equations containing the effects of surface tension and gravity are used for both fluids in the same form,

$$\nabla \cdot \mathbf{u} = s(t), \tag{1}$$

$$\frac{\partial \rho \mathbf{u}}{\partial t} + \nabla \cdot (\rho \mathbf{u} \otimes \mathbf{u}) = -\nabla p + (\nabla \cdot (\mu \nabla \mathbf{u}) + \nabla \mathbf{u} \cdot \nabla \mu) + \mathbf{F}_s - \mathbf{g} \cdot \mathbf{x} \nabla \rho + \mathbf{F}_d, \tag{2}$$

$$\frac{\partial \phi}{\partial t} + \nabla \cdot (\mathbf{u}\phi) = \phi \nabla \cdot \mathbf{u}. \tag{3}$$

where $\mathbf{u} = (u, v)$ is the velocity vector with components u and v in x and y directions respectively, p is the pressure in excess of the hydrostatic part, $\mathbf{g}$ is the gravity acceleration, ρ the density and μ the dynamic viscosity coefficient. $\mathbf{F}_s$ is the surface tension force formulated by $\mathbf{F}_s = \sigma \kappa \nabla \phi$ with σ being the surface tension coefficient and κ the interface curvature. A volume-of-fluid(VOF) function is used with an indicator function $\phi(\mathbf{x}, t)(0 \leq \phi \leq 1)$ distinguishing two kinds of fluids and the intrinsic fluid properties, such as density and viscosity, are updated based on the VOF function. It is noted that the mass source $s(t)$ and momentum source $\mathbf{F}_d$ are employed for wave generation and absorption respectively, the specific forms of which are given in following sections.

The solution of the momentum equation in interFoam is performed by constructing a predicted velocity field and then correcting it using the "Pressure Implicit with Splitting of Operators"(PISO) procedures to update the numerical solution from time level n($t = t^n$) to n+1($t = t^n + \Delta t$). To evaluate the fluxes on cell boundaries, a central differencing flux and a non-oscillatory upwind flux are adopted. When using a so-called limitedLinearV scheme, a TVD conforming flux limiter of $\psi(r) = max[0, min(2r, 1)]$ is applied to switch between two flux schemes. A numerical interface compression method is applied in interFoam to keep the interface sharp and the compression is obtained by adding a heuristic term to VOF transport equation, such that it attains,

$$\frac{\partial \phi}{\partial t} + \nabla \cdot (\mathbf{u}\phi) + \nabla \cdot [\mathbf{u}_r \phi (1 - \phi)] = \phi \nabla \cdot \mathbf{u} \tag{4}$$

And the "Multidimensional universal limiter with explicit solution"(MULES) limiter is used to limit the phase fluxes in solving VOF function. It is noted that, in this study, the divergence term $\phi\nabla\cdot\mathbf{u}$ in Eq. (4) is included in view of the fact that the mass source function turns it into a non-zero value within the source region.

The numerical framework of the present model is constructed by combining VPM and THINC/QQ schemes, which are for solving momentum equation and VOF function respectively. The projection solution procedure is employed to time advance the pressure and velocity fields and the detailed solution procedures can be found in [7]. The VPM method is applied to discretize the momentum equation, which includes the point values(PV) at cell vertices as new degrees of freedom(DOFs) in addition to the volume integrated average(VIA) and the two kinds of variables are updated separately in each time step. By adding additional DOFs, high-order reconstructions are realized over compact mesh stencil to make a significant improvement in accuracy and robustness on unstructured grids with a mild increase in computation cost. The interested readers are referred to Xie et al.(2014) [3] for more details on numerical implementation. The VOF function is computed with THINC/QQ scheme, in which a hyperbolic tangent function in the local coordinate (ξ,η,ζ) is used to approximate the indicator function $H(\mathbf{x},t)$ for the target cell Ω_i at each time step,

$$H_i(\xi,\eta,\zeta)=\frac{1}{2}(1+tanh(\beta(P_i(\xi,\eta,\zeta)+d_i))), \tag{5}$$

where β determines the steepness of the jump in the interpolation function and has a constant value of 1.5 in this study. $P_i(\xi,\eta,\zeta)=0$ represents the interface surface in the standard element, which is approximated as a curved surface by using fully quadratic polynomial that includes the geometric information. See Xie and Xiao(2017) [4] for details.

For this study, a simple base case of regular wave trains on a constant water depth $d=0.35m$ will be simulated with various numerical settings. And unless stated the numerical settings will remain in accord with the base case. The quality of simulated wave trains will be assessed in term of surface elevation. A numerical tank that measures $50\times0.5m^2$ is built with a rectangular source region($0.0667\times0.04m^2$) located at $x=5m$ and an elevation of about $1/3d$ from the still water level(SWL), a 3-meter long sponge layer is set at each end of the tank. The computational domain along with its coordinate system is shown in Fig. 1. A wave height of 0.03m and a wave period of 1.0s are taken as the wave parameters for the base case. A set of grid system with rectangular elements discretizes the entire wave tank with roughly 40 cells per

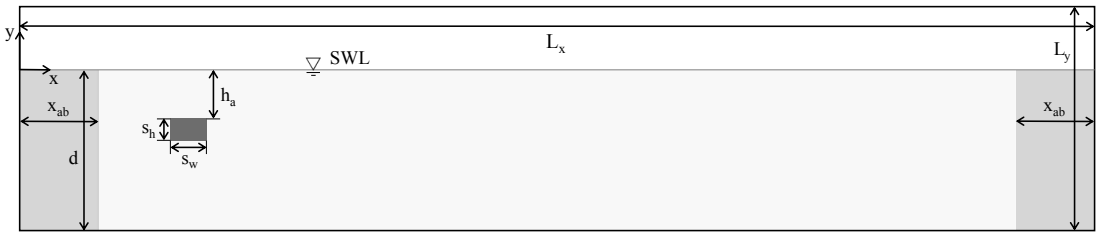

Figure 1: 2D computational domain filled with water(ivory white) and air(white), with source region(dark grey) and sponge layers(light grey).

wavelength and 10 cells per wave height in the vicinity of the SWL. The grid remains uniform in the horizontal direction but nonuniform in the vertical direction, which is coarsened gradually from the SWL to the tank bottom. The time step for reference simulation is set as $\Delta t=0.004s$, which corresponds to 250 time steps per wave period. For the generation of linear monochromatic wave trains, $\eta(t)=Hsin(\sigma t)/2$, a mass source function field will be given as,

$$s(t)=\begin{cases}\frac{CHk}{A}sin(\sigma t) & within\ source\ region\\ 0 & elsewhere\end{cases} \tag{6}$$

where C stands for the phase velocity and A is the area of the source region. A magnification factor k is applied to the mass source function for the fact that not all the momentum introduced into the system contributes to the wave generation. And according to our observation, the amplitudes of generated waves highly depend on the location of the source region relative to the SWL, so the value of factor k will be determined by making the observed wave amplitudes close enough to the desired value in this study. To prevent undesirable wave reflections from the domain boundaries, absorbing regions are employed by adding damping force $\mathbf{F}_d$ into the momentum equation, which has a form as,

$$\mathbf{F}_d=\rho\mathbf{u}A_b, \tag{7}$$

where A_b is the absorption coefficient, a commonly used form proposed by Wei and Kirby(1995) [6] is applied,

$$A_b=\begin{cases}c_\alpha\frac{e^{\left[\left(\frac{|x-x_{st}|}{x_{ab}}\right)^{n_c}\right]}-1}{e^1-1} & x_{st}<x<x_{st}+x_{ab}\\ 0 & elsewhere\end{cases} \tag{8}$$

where x_{st} and x_{ab} are the starting position and length of the absorbing regions, respectively, c_α and n_c are the empirical damping coefficients to be determined via the numerical tests, which in this study are taken as $c_\alpha=100$ and $n_c=3.5$.

It is noted that, with the present model, the steepness parameter β from the THINC function is reduced to 0.5 within the absorbing regions to enhance the absorption efficiency. Numerical experiments are conducted with both interFoam solver and the present solver, the simulated results will be compared and discussed in this section.
First, linear monochromatic wave trains which have the same setup with the base case are performed for 60 wave periods. The surface elevations along the horizontal direction after 60 wave periods are shown in Fig. 2, distinct differences between interFoam simulation and the results with the present model can be seen from this figure. This figure intuitively illustrates that the wave amplitudes in interFoam simulation diminish as the wave trains propagate farther and a nonnegligible phase shift is produced at the same time. It is noted that, though the mass source function has a form of a linear wave, the generated wave trains show nonlinearity due to the intermediate water depth condition. So the 2^{nd}-order Stokes theory is treated as the analytical results as well as what follows.

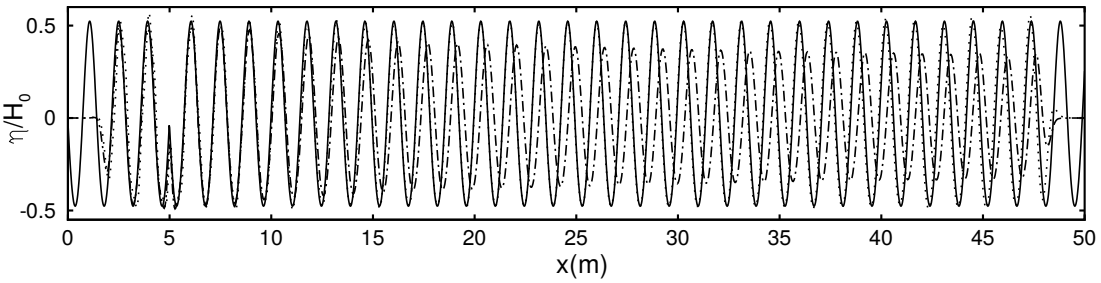

Figure 2: Surface elevations over x-location at t/T=60 with: ———, 2^{nd}-order Stokes theory; - - - - -, interFoam solver; ·····, the present solver.

Simulations are performed with different time steps and with otherwise the identical setup as the base case. A close-up view of the surface elevations recorded $10\lambda_0$ away from the source region are presented in Fig. 3a. The interFoam simulation shows that, after propagating a distance of $10\lambda_0$, significant amplitude loss and phase antedisplacement are produced in the 0.008s case. The wave profiles approach the analytical result as the time step reduces, but there is still noticeable discrepancy even with a time step of 0.0002s which roughly corresponds to a maximum Courant number of 0.01. Snapshots of the wave tank at $t/T = 60$ presented in Fig. 3b shows that interFoam simulation brings phase retrodisplacement simultaneously, which is attributed to wavelength expansion. While the present solver produces highly consistent results and the insensitivity of the present solver to time step is supposed to be attributed to the use of third-order Runge-Kutta time-integration scheme instead of first-order Euler scheme.
For the grid study, simulations are performed on two other sets of grid, one coarser grid, and one finer grid. The time steps are modified in the light of the grid size to synchronize the Courant number of the simulations. As shown in Fig. 4a and Fig. 4b, with interFoam solver, the wave amplitudes diminish, the time series of the wave profile shift forward and the wave profiles over x-location shift backward. The disparities aggravate as the coarser grid is employed. And the height loss of the simulated wave trains at the location of $10\lambda_0$ away from the source region is up to 28% of the primitive wave height H_0 on the coarsest grid. While slight differences are produced with the present solver merely when the coarsest grid is used. Something needs to be clarified is that the phase shift with the present solver is not caused by a change in wave period or wavelength as it can be observed from the start of the time series and the snapshots.
Numerical simulations of free-surface waves are carried out with both open-source code interFoam and the present model based on VPM and THINC/QQ methods. A mass source function and a sponge layer are employed to generate wave trains from the inner field and absorb the generated waves near the tank boundaries. Main attention has been paid to the numerical dissipation along the propagation direction of the wave trains. By examining the surface elevations at the location of several wavelengths away from the source region, numerical dissipation is evaluated in the terms of wave amplitude and phase consistency. It has been shown that great numerical dissipation is produced with interFoam solver as wave amplitude loss and phase shift can be observed in interFoam simulations. And the dissipation enlarges as coarser grid solutions and larger time steps are adopted. On the other hand, the results obtained by the present model are insensitive to the temporal and spatial discretization in our time step and grid studies which show a great advantage in wave energy preservation. Future research will focus on the simulation performance of surface-waves with different wave periods and wave steepness in light of that the relatively higher-frequency waves and steeper waves are supposed to suffer from greater numerical dissipation. Although only structured grids are employed in this study, the present numerical framework can be straightly applied on unstructured grids with arbitrary and hybrid elements, which makes it potentially useful and efficient for applications involving complex geometrical configurations such as wave-structure interactions and wave deformation.

Acknowledgments

This study was partially supported by the National Natural Science Foundation of China (Grant No. 35351679212), Zhejiang Provincial Natural Science Foundation of China (Grant No. LR16E090002).

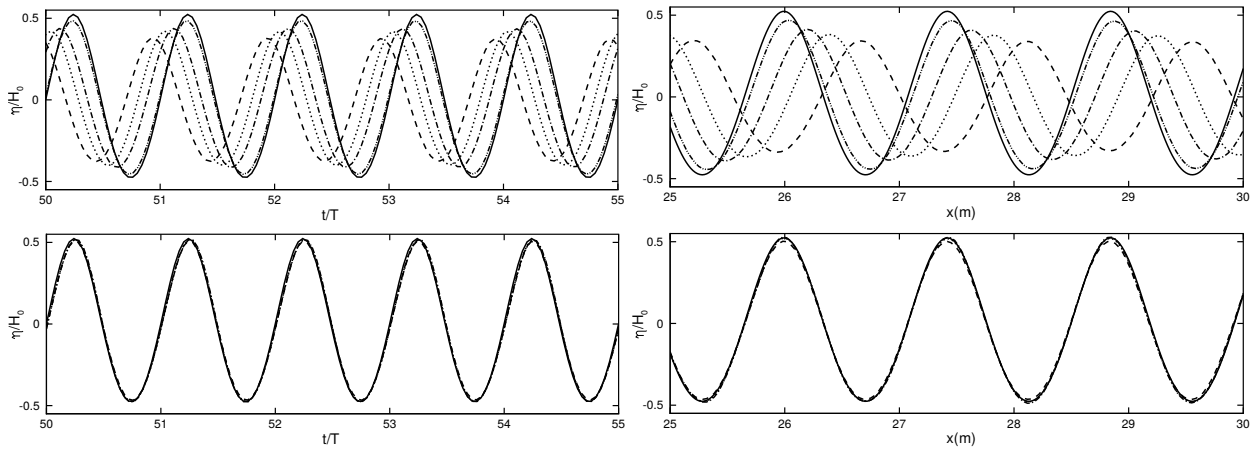

(a) over time recorded $10\lambda_0$ away from source region **(b) over x-location at $t/T = 60$**

Figure 3: Surface elevations for different time steps: ———, 2^{nd}-order Stokes theory; - - - - -, 0.008s; ·····, 0.004s; -·-·-·-, 0.002s; -··-··-··-, 0.0002s, with interFoam solver(top) and the present solver(bottom)

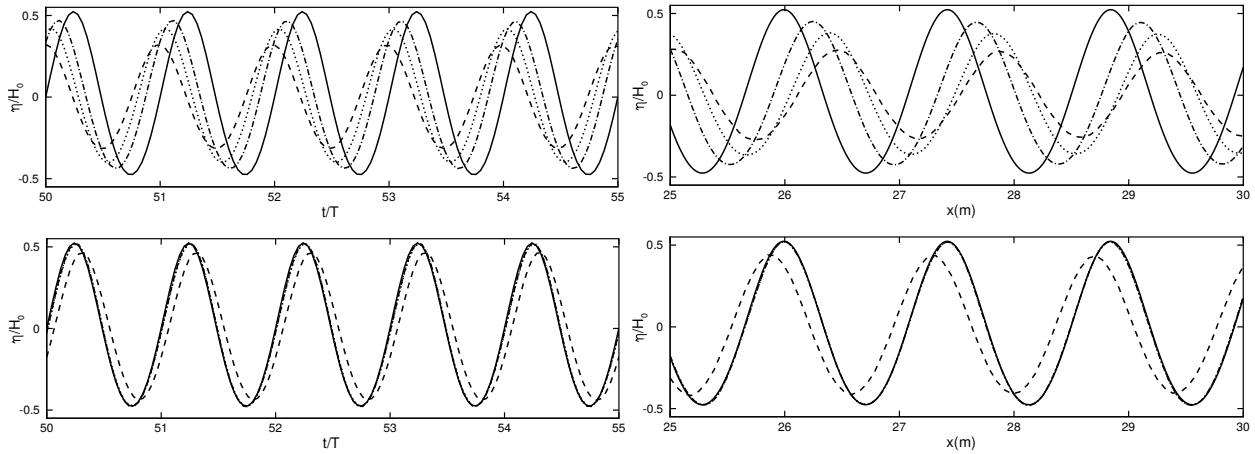

(a) over time recorded $10\lambda_0$ away from source region **(b) over x-location at $t/T = 60$**

Figure 4: Surface elevations for different grid resolutions: ———, 2^{nd}-order Stokes theory; - - - - -, 2 times coarser grid; ·····, reference grid; -·-·-·-, 2 times finer grid, with interFoam solver(top) and the present solver(bottom).

References

[1] J.-J. Cha and D.-C. Wan, "Numerical wave generation and absorption based on openfoam," *Ocean Engineering(Haiyang Gongcheng)*, vol. 29, no. 3, pp. 1–12, 2011.

[2] R. Perić and M. Abdel-Maksoud, "Generation of free-surface waves by localized source terms in the continuity equation," *Ocean Engineering*, vol. 109, pp. 567–579, 2015.

[3] B. Xie, S. Ii, A. Ikebata, and F. Xiao, "A multi-moment finite volume method for incompressible navier–stokes equations on unstructured grids: volume-average/point-value formulation," *Journal of Computational Physics*, vol. 277, pp. 138–162, 2014.

[4] B. Xie and F. Xiao, "Toward efficient and accurate interface capturing on arbitrary hybrid unstructured grids: The thinc method with quadratic surface representation and gaussian quadrature," *Journal of Computational Physics*, vol. 349, pp. 415–440, 2017.

[5] P. Lin and P. L.-F. Liu, "Internal wave-maker for navier-stokes equations models," *Journal of waterway, port, coastal, and ocean engineering*, vol. 125, no. 4, pp. 207–215, 1999.

[6] G. Wei and J. T. Kirby, "Time-dependent numerical code for extended boussinesq equations," *Journal of Waterway, Port, Coastal, and Ocean Engineering*, vol. 121, no. 5, pp. 251–261, 1995.

[7] B. Xie, P. Jin, and F. Xiao, "An unstructured-grid numerical model for interfacial multiphase fluids based on multi-moment finite volume formulation and thinc method," *International Journal of Multiphase Flow*, vol. 89, pp. 375–398, 2017.